

Submitted to The Astrophysical Journal

HIGH TEMPERATURE PHOTOCHEMISTRY IN THE ATMOSPHERE OF HD189733B

Running Head: PHOTOCHEMISTRY ON HD189733B
M. R. Line¹, M. C. Liang², Y. L. Yung¹

¹Division of Geological and Planetary Sciences, California Institute of Technology, Pasadena, CA, 91125, USA

²Research Center for Environmental Changes, Academia Sinica, Taipei, Taiwan

³Graduate Institute of Astronomy, National Central University, Jhongli, Taiwan

⁴Institute of Astronomy and Astrophysics, Academia Sinica, Taipei, Taiwan

Corresponding Author Email: mrl@gps.caltech.edu

ABSTRACT

Recent infrared spectroscopy of hot exoplanets is beginning to reveal their atmospheric composition. Deep within the planetary atmosphere, the composition is controlled by thermochemical equilibrium. Photochemistry becomes important higher in the atmosphere, at levels above ~ 1 bar. These two chemistries compete between ~ 1 -10 bars in hot Jupiter-like atmospheres, depending on the strength of the eddy mixing and temperature. HD189733b provides an excellent laboratory in which to study the consequences of chemistry of hot atmospheres. The recent spectra of HD189733b and HD209458b contain signatures of CH_4 , CO_2 , CO and H_2O . Here we identify the primary chemical pathways that govern the abundances of CH_4 , CO_2 , CO and H_2O in the cases of thermochemical equilibrium chemistry, photochemistry, and their combination. Our results suggest that the abundance of these species can be photochemically enhanced above or below the thermochemical equilibrium value, so some caution must be taken when assuming that an atmosphere is in strict thermochemical equilibrium.

Key words: atmospheric effects - methods: numerical – planetary systems - planets and satellites: atmospheres – stars: individual (HD189733b) – planetary systems – radiative transfer

1. INTRODUCTION

1
2 Of the more than four hundred exoplanets discovered thus far, only a small number are transiting
3 hot exoplanets, dubbed “hot Jupiters”, from which we can obtain limited spectral information. A
4 variety of chemical species have been detected in hot Jupiter atmospheres. These include atomic
5 species like sodium (Na) (Charbonneau et al. 2002), atomic hydrogen (Vidal-Madjar et al. 2003),
6 atomic carbon and oxygen (Vidal-Madjar et al., 2004), and the molecular species: CO, CO₂,
7 H₂O and CH₄ (Tinetti et al. 2007; Swain et al. 2009a, 2009b). The detection of these species
8 allows us to begin to explore the chemical pathways that control the observed abundances of
9 these species. The species so far identified suggest that hydrocarbon chemistry via CH₄
10 photolysis as well as oxygen and water reactions are important.

11
12 The primary chemical pathways that determine chemical abundances in our own solar system are
13 classified as due to either thermoequilibrium chemistry or photochemistry. Ion chemistry may
14 also be important in these hot, highly irradiated atmospheres as it is important in the upper
15 atmospheres of our own solar system planets (Vuitton et al. 2009; Kim & Fox 1994; Friedson et
16 al. 2005). Current atmospheric modeling of hot Jupiter atmospheres typically assume an
17 atmospheric chemical composition consistent with thermochemical equilibrium (Sharp &
18 Burrows 2006; Showman et al. 2009; Burrows et al. 1997; Fortney et al. 2005; Fortney et al.
19 2010; O’Donovan et al. 2010; Rogers et al. 2009; Marley et al. 2007). Photochemical or other
20 disequilibrium mechanisms, such as quenching, have not received the same attention. (See,
21 however, Cooper & Showman 2006; Zahnle et al. 2009; Liang et al. 2003, 2004).
22 Thermoequilibrium chemistry occurs in high temperature and pressure regimes where chemical
23 timescales are short, typically deep within the atmospheres of giant planets (~1000 bars).

24 Abundances are determined solely by the thermodynamic properties of compounds in the system
25 via the minimization of the Gibbs free energy (Yung & DeMore 1989). Photochemistry is a
26 disequilibrium process due to UV alteration by the host star. Photochemistry therefore should be
27 important in hot-Jupiter atmospheres, given their proximity to their host stars (Liang et al. 2003).

28

29 Liang et al. (2003) were the first to explore the photochemistry that may occur on highly
30 irradiated giant planets through modeling the sources of atomic hydrogen in HD209458b.
31 However, some of the rate coefficients used in that study are
32 unsuitable for these high-temperature regimes, and several key reactions governing the
33 production and loss of H₂O and CO₂ were not included. Additionally, better estimates of
34 temperature and vertical mixing profiles can be obtained from more sophisticated GCM
35 simulations.

36

37 Zahnle et al. (2009) explored products of sulfur photochemistry and how they may be
38 responsible for the strong UV absorbers that cause thermal inversions as well as the formation of
39 hydrocarbon soot. So far there have been no detections of sulfur species on these hot Jupiters.

40

41 The goal of this investigation is to understand the chemistry that produces the observed
42 abundances of $\sim 10^{-4}$, $\sim 10^{-6}$, $\sim 10^{-4}$, and $\sim 10^{-7}$ for CO, CO₂, H₂O and CH₄, respectively, as
43 detected in the dayside emission spectrum of HD189733b (Swain et al. 2009a) by combining
44 separate photochemical and thermochemical models and then comparing the results to
45 simulations using photochemistry/thermochemistry alone. Furthermore, it has been recently
46 suggested by Madhusudhan & Seager (2009) that there may be as much as 700 ppm of CO₂

47 present in the atmosphere of HD189733b. The discrepancy between this value and the value
48 from Swain et al. (2009a) is due to the assumed vertical distribution of CO₂ in the atmosphere
49 (constant, versus high concentration at one pressure level), which is not well constrained. This
50 discrepancy suggests that there is much degeneracy in retrieving temperature and mixing ratio
51 profiles, and that the exact values of the mixing ratios, or their vertical distributions, of the
52 detected species are not well known. In this study, we identify the important mechanisms that
53 govern the abundance of these detected species and their vertical distribution, using HD189733b
54 as an example.

55

56

2. MODELING

57 We use both a thermochemical model and a photochemical model to explain the observed
58 abundances of CO, CO₂, H₂O and CH₄ in the atmosphere of HD189733b. We want to
59 understand the effects that temperature and eddy mixing have on the photochemically derived
60 mixing ratios. We adopt a hot profile representative of dayside temperatures and cool profile
61 representative of night-side temperatures for 30° N from Showman et al. (2009) (Figure 1). We
62 assume isothermal profiles above the upper boundary of the Showman et al. (2009) GCM for the
63 sake of simplicity. These two profiles appear to have a thermal inversion near 1 mbar with a
64 day-night contrast of ~500 K. The use of two T-P profiles will illuminate the day/night contrast
65 of the modeled species. Though HD189733b is not expected to have an inversion, we still
66 choose these T-P profiles because they span the range of hot Jupiter temperature profiles in the
67 literature (Fortney et al. 2006; Tinetti et al. 2007; Burrows et al. 2008), and the existence of an
68 inversion does not significantly affect the major chemical pathways.

69

70 In order to determine the thermoequilibrium abundances we use the Chemical Equilibrium with
71 Applications model developed by Gordon & McBride (1994). These abundances at the
72 appropriate lower boundary (explained later) will be used for our lower mixing ratio boundary
73 condition in the photochemical model. Thermochemical calculations require only pressure and
74 temperature along with the relative molar mixing ratios of the atomic species involved in the
75 compounds of interest, in this case C, O and H (no N or S because they have not yet been
76 detected). For the sake of simplicity, and in the absence of any other information, we assume
77 solar abundance of these species ($[C]/[H] \sim 4.4 \times 10^{-4}$, $[O]/[H] \sim 7.4 \times 10^{-4}$, where $[i]$ denotes the
78 concentration of species i (Yung & DeMore 1999 pg. 112). The thermochemical model
79 computes the abundances of all possible compounds formed by those atomic species via a Gibbs
80 Free energy minimization routine (Gordon & McBride 1994). We compute the equilibrium
81 abundances at each pressure-temperature level for our chosen temperature profiles. We would
82 expect to see thermochemical equilibrium abundances in an atmosphere that is not undergoing
83 any dynamical or photochemical processes, or where chemical timescales are much shorter than
84 any disequilibrium timescales (Cooper & Showman 2006; Prinn & Barshay 1977; Smith 1998).
85
86 To compute the photochemical abundances of the species of interest, we use the Caltech/JPL-
87 Kinetics 1D photochemical model (Allen et al. 1981; Moses et al. 2005; Gladstone et al. 1996;
88 Yung et al. 1984) for HD189733b. HD189733b is in a 2.2 day period orbiting at 0.03 AU
89 around a K2V star. We use the UV stellar spectrum from HD22049 which is also a K2V star
90 (Segura et al. 2003). The model computes the abundances for 32 species involving H, C and O
91 in 258 reactions including 41 photolysis reactions and includes both molecular and eddy
92 diffusion. The model uses the same hydrocarbon and oxygen chemistry as in Liang et al. (2003)

93 and Liang et al. (2004) but with high temperature rate coefficients for the key reactions involved
94 in the production and loss of H, CH₄, CO₂, CO, OH and H₂O. The reaction rates given in the
95 remainder of this paper are taken from Baulch et al. (1992) unless otherwise noted. We have
96 also added two key reactions involved in the destruction of H₂O and CO₂. We have not,
97 however, added a complete suite of reactions in order to achieve thermochemical equilibrium
98 kinetically (e.g., Visscher et al. 2010). We do not expect this omission to invalidate our results,
99 as we have included the key chemical pathways that govern the production and loss of the
100 species of interest. The model atmosphere for the photochemical model uses the two temperature
101 profiles described above. The lower boundary of the photochemical model is important in
102 determining the mixing ratios throughout the atmosphere. We will estimate this lower boundary
103 using quench level arguments rather than arbitrarily choosing some level. For more details on
104 quench level estimation we refer the reader to Cooper & Showman (2009), Smith (1998) and
105 Prinn & Barshay (1977).

106
107 Eddy and molecular diffusion are key parameters determining the distribution of the abundances
108 in the atmosphere. Eddy diffusion is the primary vertical transport mechanism in our 1D model.
109 The strength of vertical mixing will determine where in the atmosphere the species become
110 chemically quenched, and thus defines the lower boundary conditions for the photochemical
111 model (Prinn & Barshay 1977; Smith 1997). Following Prinn & Barshay (1977), the transport
112 timescale is given by

113
$$\tau_{trans} \cong \frac{L^2}{K_z} \quad (1)$$

114 where L is a vertical length scale typically chosen to be the scale height and K_z is the eddy
115 diffusion coefficient. The chemical loss timescale of species i is given by

116
$$\tau_{chem,i} = \frac{[i]}{L_i} \quad (2)$$

117 where $[i]$ is the concentration of species i and L_i is the loss rate of species i , typically determined
 118 by the bottleneck reaction. The quench level for species i is defined where $\tau_{trans} = \tau_{chem,i}$. For
 119 levels where $\tau_{trans} < \tau_{chem,i}$ the mixing ratio of species i is fixed at the quench level value. For
 120 levels below the quench level, the compounds reach chemical equilibrium.

121
 122 In order to determine the quench level in the atmosphere HD189733b, we must first estimate the
 123 strength of eddy mixing and the timescale for the conversion of CO to CH₄ (Griffith & Yelle
 124 1999; Prinn & Barshay 1977). The eddy diffusion profile adopted in this model is derived from
 125 a globally RMS-averaged vertical wind profile from a GCM (Showman 2010 private
 126 communication) and is estimated by

127
$$K_z \sim wL \quad (3)$$

128 where w is the RMS-averaged of the vertical wind velocity. Smith (1998) suggests that the
 129 appropriate length scale is some fraction of the scale height. Here we assume that it is the scale
 130 height, thus giving us an upper limit on eddy diffusion. The GCM derived RMS-averaged
 131 vertical winds range from 0 (at ~200 bars) to 7 m/s (~0.8 mbars). The vertical wind is assumed
 132 to be constant above this height. Combining this with a typical scale height of ~200 km gives an
 133 eddy diffusion of $\sim 10^{10}$ cm² s⁻¹ (Figure 1). Typical transport timescales from (1) are on the order
 134 of $\sim 10^5$ s.

135
 136 The rate-limiting step in the conversion of CO to CH₄, and thus the reaction determining the
 137 chemical lifetime of CO, is



139 (Yung et al. 1988; Griffith & Yelle 1999; Cooper & Showman 2006). The rate coefficient in
 140 reaction 4 has not been measured in the lab, but its reverse reaction rate has been measured to be:

$$141 \quad k_r = 1.4 \times 10^{-6} T^{-1.2} e^{-7800/T} \text{ cm}^6 \text{ s}^{-1} \quad (5)$$

142 where T is the temperature at which the reaction takes place (Page et al. 1989). The forward
 143 reaction rate, k_f can be estimated via

$$144 \quad \frac{k_f}{k_r} = K_{eq} = e^{(G_f - G_r)/RT} \quad (6)$$

145 where K_{eq} is the equilibrium constant for the net thermochemical reaction (Yung et al. 1988)



147 where G_f and G_r are the Gibbs free energies of the reaction, given respectively by
 148 $H[\text{H}] + H[\text{H}_2\text{CO}] - T(S[\text{H}] + S[\text{H}_2\text{CO}])$ and $H[\text{CH}_3\text{O}] - TS[\text{CH}_3\text{O}]$ with $H[\text{X}]$ being the enthalpy of
 149 formation of species X and $S[\text{X}]$ being the entropy of species X. The enthalpies and entropies of
 150 the given species can be found in Yung & DeMore (1999) pg 58. With the relevant
 151 thermochemical data and equations (5) and (6) we can estimate the forward reaction rate of
 152 reaction (4) to be

$$153 \quad k_f = 5.77 \times 10^{-12} T^{-1.2} e^{3327/T} \quad (8)$$

154 The CO chemical lifetime can then be determined using:

$$155 \quad \tau_{chem} \sim \frac{[\text{CO}]}{k_f [\text{H}][\text{H}_2\text{CO}]} \quad (9)$$

156 where the concentrations of CO, H and H₂CO are determined via the thermochemical model.
 157 Upon equating (9) with (1) using the dayside temperature profile we determine the quench level,
 158 and thus the lower boundary to be ~3 bars (~1530 K) which is similar to the results of Cooper &
 159 Showman (2006) for HD209458b. This pressure level is much higher than that of Jupiter (~100
 160 bars) (Prinn and Barshay 1977) and is similar to that of brown dwarfs (~6 bars) (Griffith & Yelle

161 1999). Choosing a length scale less than the scale height as suggested by Smith et al (1998) can
162 move the quench level to a higher pressure. This is because the chemical timescale in equation 9
163 increases with increasing altitude and lower temperature. Using a length scale of $0.1H$ instead of
164 H moves the quench level to ~ 8 bars, at where there is very little change in the thermochemical
165 mixing ratios from ~ 3 bars (Figure 2). Additionally, there is no significant difference in quench
166 level between the nightside and dayside because the two T-P profiles converge near the quench
167 level.

168

169 We assume a zero concentration gradient at the lower boundary in order to allow photochemical
170 products to sink down into the deeper atmosphere except for the observed species of CO, H₂O,
171 CH₄, CO₂. For these species we fix the mixing ratios to be the thermochemically-derived values
172 at the ~ 3 bar quench level: 8.41×10^{-4} , 6.36×10^{-4} , 4.09×10^{-5} , and 1.96×10^{-7} , respectively, for the
173 dayside and 8.39×10^{-4} , 6.38×10^{-4} , 4.25×10^{-5} , and 1.98×10^{-7} , respectively, for the nightside. We
174 assume a zero flux boundary condition for the top of the atmosphere e.g, little or no atmospheric
175 escape, though this assumption may not be entirely true for atomic hydrogen (Vidal-Madjar et al.
176 2003). This assumption has a negligible effect on the results.

177

178

3. RESULTS

179

3.1 Thermochemical Results

180

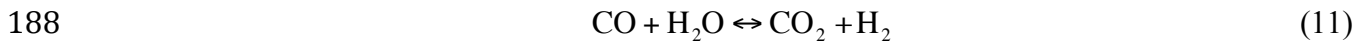
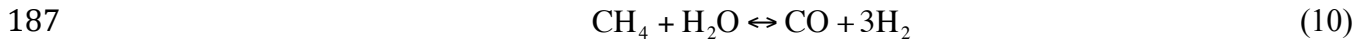
181

182

183

The thermochemically derived mixing ratios (relative to H₂) are shown in Figure 2. Again, these
are the expected mixing ratios if there were no dynamical or photochemical process occurring in
the atmosphere, which we know not to be true. If we focus first on the dayside profiles, we can
see that CO is the dominant carbon bearing species and remains relatively constant with altitude

184 as do H₂O and CO₂. We also notice that CH₄ falls off rapidly with increasing altitude
185 (decreasing pressure). We can understand this result by noting that CO, CH₄ and H₂ abundances
186 are related through the net thermochemical reactions



189 Then by Le Chatelier's principle, as the total partial pressure of the atmosphere decreases, the
190 system will want to resist that decrease in order to maintain equilibrium by producing more
191 molecules (smaller molecules), which in this case results in the production of CO and H₂. Upon
192 comparing the dayside profiles to the cooler nightside profile, we notice that CH₄ becomes more
193 abundant. CH₄ is more energetically favorable at lower temperatures and is much more sensitive
194 to the effects of temperature than CO and CO₂. We also note that atomic hydrogen is more
195 abundant at warmer temperatures than at cooler temperatures due to the entropy term in the
196 Gibbs free energy. From a thermochemical perspective, we can expect ~10 mbar mixing ratios
197 of the observable species, CO, H₂O, CH₄ and CO₂ to range from: (2-9)×10⁻⁴, (6-13) ×10⁻⁴, (2.6-
198 6758) ×10⁻⁷, (4.7-16) ×10⁻⁷, respectively, due to the day/night contrast. For comparison, the
199 measured dayside emission values from Swain et al (2009a) for CO, H₂O, CH₄ and CO₂ are
200 respectively, ~10⁻⁴, ~10⁻⁴, ~10⁻⁷, and ~10⁻⁶

201

202

3.2 Photochemical Results

203

204

205

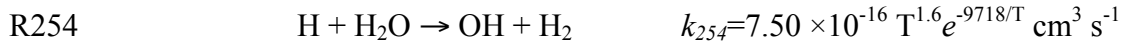
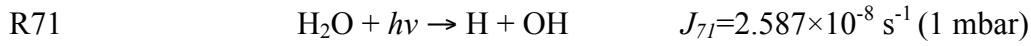
206

We run four cases of our photochemical model (Figure 3) in order to compare the effects of
temperature and photolysis versus no photolysis on the mixing ratios (relative to H₂) for H, CO,
H₂O, CO₂ and CH₄. In the following subsections we will discuss the important reactions
governing the production and loss of each of the relevant species.

207
208
209
210
211
212
213
214
215
216
217
218
219
220
221
222
223
224
225
226
227
228
229

3.2.1 H₂O, OH, and H

The primary reactions that govern the production and loss of H₂O are



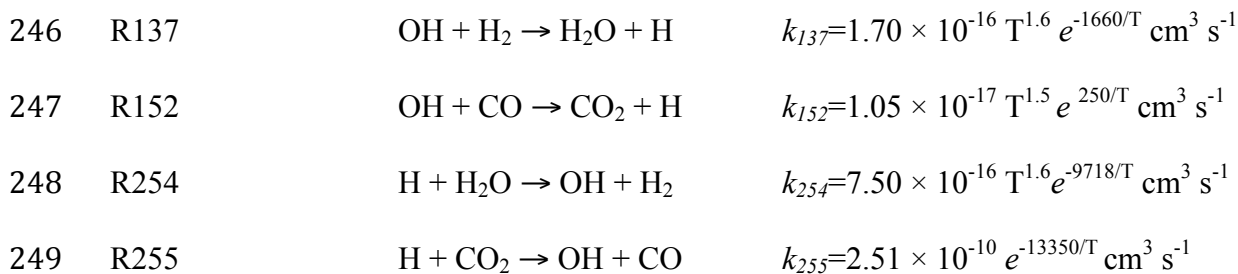
R137 and R254 are fast enough to readily recycle each other so that the abundance of H₂O remains relatively constant with altitude at the quench level value of $\sim 6.36 \times 10^{-4}$ below the homopause at ~ 10 nbar. The photolysis of H₂O does not significantly affect its abundance in the observable atmosphere as can be seen in Figure 3, because the loss timescale of H₂O when struck by photolysis is everywhere longer than the transport timescale, thus allowing recently photolyzed parcels to be readily replenished by upwelling. The photolysis of H₂O, however, does produce the important OH and H radicals that drive the remainder of the chemistry (Figure 4), with the net result being the conversion of H₂ to 2H.

H₂O photodissociates into OH and H at wavelengths lower than 2398 Å. For HD189733b below this wavelength there are $\sim 8 \times 10^{15}$ photons $\text{cm}^{-2} \text{ s}^{-1}$ available for H₂O photolysis. For comparison, the UV flux below this wavelength at Jupiter is $\sim 3 \times 10^{14}$ photons $\text{cm}^{-2} \text{ s}^{-1}$ and for HD209458b, $\sim 3 \times 10^{18}$ photons $\text{cm}^{-2} \text{ s}^{-1}$. OH and H increase with increasing altitude due to the availability of more UV photons. The production of H at high altitudes via H₂O photolysis may be the driver of hydrodynamic escape on hot Jupiters (Liang et al. 2003).

230 In short, the abundance of H₂O is primarily set by the thermochemical equilibrium value at the
 231 lower boundary condition, taken here to be the quench level, and rapidly decreases with altitude
 232 above the homopause. If the quench level changes, the observable value of H₂O will change but
 233 not significantly, as can be seen in Figure 2. The derived value here is slightly higher than the
 234 Swain et al. 2009a dayside emission observations of $(0.1-1) \times 10^{-4}$ but is more consistent with the
 235 value obtained by the Tinetti et al. 2007 terminator observations of $\sim 5 \times 10^{-4}$. The day to night
 236 contrast is nearly unnoticeable in Figure 3.

238 3.2.2 CO & CO₂

239 Thermochemically, CO is the dominant carbon reservoir in hot atmospheres above ~ 10 bars
 240 (Figure 2). The abundance of CO is set by the quench level thermochemical equilibrium
 241 abundance of 8.4×10^{-4} . The abundance of CO₂ is determined via the interconversion of oxygen
 242 from the large reservoirs of CO and H₂O into CO₂ via the OH radical. Deeper down in the
 243 atmosphere, say, below the quench level, or in the presence of weak vertical transport (low eddy
 244 diffusion), oxygen is moved into CO₂ via the following reactions



250
 251 R152 is the reaction that gives the oxygen from H₂O and CO to CO₂. There is no net production
 252 or loss of species from these reactions, meaning they will assume thermochemical equilibrium.

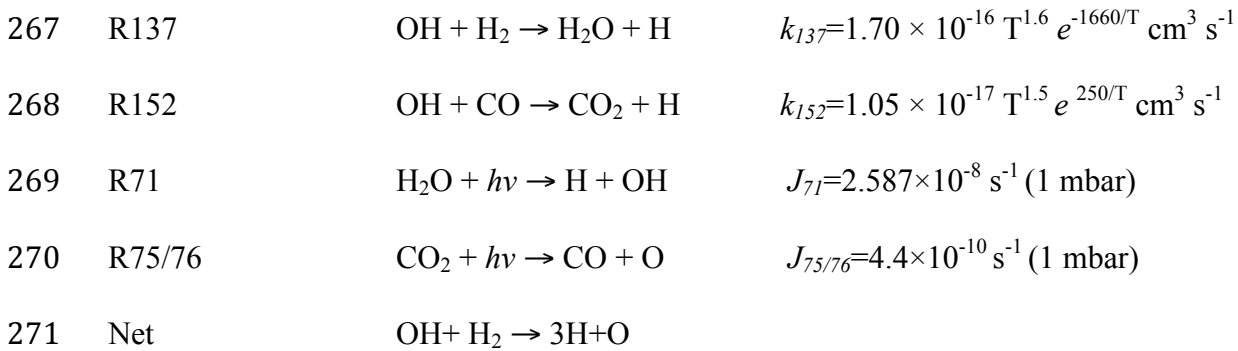
253 Assuming steady state, these 4 reactions can be combined to give the kinetically achieved
 254 thermochemical mixing ratio of CO₂ in terms of the rate constants (*k*) and mixing ratios (*f*) of the
 255 large reservoirs of CO and H₂O

$$256 \quad f_{CO_2} \sim \frac{k_{152}k_{254}}{k_{137}k_{255}} f_{H_2O} f_{CO} \quad (12)$$

$$257 \quad = 1.85 \times 10^{-7} T^{1.5} e^{5542/T} f_{H_2O} f_{CO}$$

258 This relation would determine the mixing ratio of CO₂ in the absence of any disequilibrium
 259 mechanisms such as photochemistry or quenching. Using the thermochemical mixing ratios of
 260 H₂O (~6×10⁻⁴) and CO (~9×10⁻⁴) and evaluating the rate constants at the daytime temperature
 261 (T~1200 K) we obtain a CO₂ mixing ratio of ~4×10⁻⁷ which is consistent with Figure 2.

262
 263 In the photochemical limit (in the absence of eddy mixing), the photolysis reactions, R71 and
 264 R75 become more important and effectively replace R254 and R255, so the important chain of
 265 reactions becomes:



272
 273 Combining these reactions allows us to estimate the photochemical mixing ratio of CO₂ with

$$274 \quad f_{CO_2} \sim \frac{k_{152}J_{71}}{k_{137}J_{75+76}} f_{H_2O} f_{CO} \quad (13)$$

275
$$= 0.062T^{-0.1}e^{1910/T} \frac{J_{71}}{J_{75+76}} f_{H_2O} f_{CO}$$

276 where J is the photolysis rate of the indicated photolysis reaction. As an extreme case we
 277 assume the top of atmosphere photolysis rate of H_2O is $\sim 10^{-5} s^{-1}$, the photolysis rate of CO_2 is
 278 $\sim 5 \times 10^{-8} s^{-1}$, and the dayside temperature is ~ 1200 K, giving an upper limit of $\sim \text{few} \times 10^{-5}$ for
 279 f_{CO_2} . Equation 13 suggests that the abundance of CO_2 is photochemically enhanced rather than
 280 reduced. The abundance of CO_2 in the presence of only quenching (no photochemistry) will
 281 remain fairly constant below the homopause at ~ 1 nbar (Figure 3). This is due to the lack of
 282 excess OH produced in R71 used to drive R152 to produce CO_2 . Again, for comparison, the
 283 observed mixing ratio of CO_2 from Swain et al. (2009a) is $\sim 10^{-7}$ - 10^{-6} .

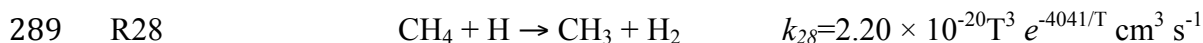
284

285

3.2.3 CH_4 and Heavier Hydrocarbons

286 The primary fate of CH_4 in the upper atmosphere is reaction with H to produce CH_3 , which
 287 immediately reacts with H_2 to restore CH_4 ,

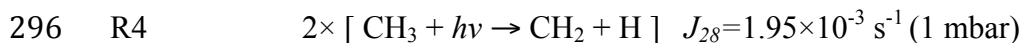
288



291

292 The result is a closed loop. However, the above recycling is not perfect, and the following
 293 sequence of reactions occur in the upper atmosphere

294



298 Net $2\text{CH}_4 \rightarrow \text{C}_2\text{H}_2 + 2\text{H}_2 + 2\text{H}$

299

300 The net result is production of C_2H_2 in the upper atmosphere at the ~ 1 ppm level. No other C_2
301 hydrocarbons are produced in significant quantities. The primary fate of C_2H_2 from the upper
302 atmosphere is downward transport, followed by hydrogenation back to CH_4 . The abundance of
303 CH_4 is $\sim 4 \times 10^{-5}$, which is several order of magnitudes larger than the $\sim 10^{-7}$ detected by Swain et
304 al (2009) and used by Liang et al. (2003).

305

306

4. DISCUSSION

307 We have analyzed the important disequilibrium mechanisms, photochemistry and simple
308 dynamical quenching that govern the vertical distribution of the observed species in hot Jupiter
309 atmospheres. With the exception of methane, our derived abundances are consistent with the
310 observations of Swain et al. (2009a). We obtained a value of $\sim 4 \times 10^{-5}$, while the observations
311 suggest two orders of magnitude less. The observed value of $\sim 10^{-7}$ corresponds to the
312 thermochemical equilibrium value at ~ 10 mbars. This would mean the quench level would have
313 to be at this pressure, suggesting an eddy diffusion on the order of $\sim 10^3 \text{ cm}^2 \text{ s}^{-1}$ from equations
314 (9) and (1). Alternatively, it may be possible that the observations are probing above the
315 homopause where the mixing ratio can be substantially less than $\sim 10^{-5}$ (Figure 3). Line lists
316 used in radiative transfer models are also not well known and are constantly changing at these
317 high temperatures which can play a significant role in dictating the retrieved abundances from
318 the observations (Tinetti 2010 private communication). Our value of methane is also several
319 orders of magnitude larger than reported by Liang et al. (2003) for HD209458b. This is because
320 the temperature at the lower boundary used in Liang et al. (2003) for HD209458b is ~ 700 K

321 hotter than our lower boundary temperature of ~ 1530 K and methane is less stable at higher
322 temperatures.

323
324 The metallicity of these hot Jupiters is not well constrained. Swain et al. (2009a) suggests that
325 the metallicity for HD189733b may be subsolar and that the $[C]/[O]$ ratio is between 0.5 and 1.
326 We assumed solar metallicity, but we can explore what might happen if this is not the case.
327 Changes in metallicity will affect the thermochemical equilibrium abundances. This will in turn
328 change the lower boundary mixing ratios. We varied the metallicity (taken here to be
329 $([C]+[O])/[H]$) from one tenth solar up to ten times solar to see what effect it would have on our
330 lower boundary mixing ratios (Figure 6). The thermochemical mixing ratios of CO, H₂O and
331 CO₂ vary by several orders of magnitude over the range of metallicities, where as CH₄ changes
332 very little. This orders of magnitude change at the lower boundary due to metallicity will affect
333 our photochemical results by the same amount. With ten times the solar metallicity we could
334 expect mixing ratios of CO and H₂O to be as high as ~ 0.1 and CO₂ as high as 10^{-5} . CO₂ is more
335 readily affected by metallicity than the other species because it has two oxygen's as opposed to
336 CO's one oxygen. Even higher metallicities will produce more extreme abundances of CO, CO₂
337 and H₂O.

338
339 The $[C]/[O]$ ratio, also affects the thermochemical abundances. Here we vary the $[C]/[O]$ ratio
340 from 0.1 to 10 times the solar ratio of ~ 0.6 while keeping the overall metallicity $([C]+[O])/[H]$
341 constant at the solar value (Figure 6). The mixing ratio of CO does not vary significantly, but
342 can get as high as $\sim 10^{-3}$ given a slightly super solar $[C]/[O]$ ratio. CO₂ rapidly decreases for
343 ratios above solar and can get as low as 0.1 ppb for 10 times the solar ratio. As the $[C]/[O]$ ratio

344 increases past 1, H₂O and CH₄ swap roles in taking up H and can change as much as 3 orders of
345 magnitude.

346

347 There appears to be minor compositional variability between the nightside and dayside.
348 Comparing the solid curves in the top of Figure 3 to the dashed curves in the bottom of Figure 3
349 gives some sense of the magnitude of the day-night variability. There are no dissociating
350 photons on the nightside, so the quench level mixing and atmospheric circulation determine the
351 abundance throughout the rest of the atmosphere below the homopause. There is a less than 1%
352 maximum variability in CO and H₂O, a factor of ~3 more CH₄ on the nightside over the dayside
353 and up to a factor of 2 more CO₂ on the dayside. CO₂ and CH₄ concentrations experience more
354 variability, because they are most affected by photochemical reactions that only occur on the
355 dayside (CH₄ gets destroyed due to R141 and photolysis, CO₂ enhanced via equation 13). C₂H₂
356 would exhibit much variability since it is produced strictly from photochemistry. We could
357 expect to see up to 1 ppm on the dayside of these hot planets with very minute amounts on the
358 nightside where it would be readily thermochemically recycled back to methane. Terminator
359 observations should fall somewhere between the dayside and nightside values.

360

361

5. CONCLUSIONS

362 We have shown that both photochemistry and vertical quenching can significantly alter the
363 abundances of CO₂, CH₄ and C₂H₂ in hot Jupiter atmospheres. Vertical quenching determines
364 the lower boundary values and thus the mixing ratios of CO and H₂O, which are not significantly
365 affected photochemically. CO₂ can be photochemically produced above its quench level value
366 by the reaction described in equation (13), and CH₄ can be readily photochemically destroyed.

367 These ideas can be extended to other hot Jupiter atmospheres, though we used HD189733b as
368 our test case. One can see from equation (13) that the fate of CO₂ is determined by the
369 temperature of the atmosphere, and the ratio of the H₂O photolysis rate to the CO₂ photolysis rate
370 which all depend on the stellar type and the distance. Knowledge of these terms will allow us to
371 predict the abundance of CO₂ in any hot Jupiter atmosphere. Finally, the vertical distribution of
372 species derived from thermochemical equilibrium can deviate substantially from those derived
373 via quenching, photochemistry and diffusion, and the simple assumption of thermochemical
374 equilibrium may not be valid in the observable regions of these atmospheres.

375

376 **ACKNOWLEDGEMENTS**

377

378 We especially thank Adam Showman for providing us his GCM outputs for temperature and
379 vertical winds making it possible for us to determine the eddy diffusion coefficient both of which
380 form the basis of our model atmosphere. We also thank Run-Li Shia, Giovanna Tinetti, Xi
381 Zhang, Konstantin Batygin, Mimi Gerstell, Chris Parkinson, Vijay Natraj, Kuai Le, Mark Swain,
382 Julie Moses, Wes Traub, Pin Chen, Gautam Vasisht, Nicholas Heavens, Heather Knutson, Sara
383 Seager and the Yuk Yung group for very useful discussions and reading the manuscript. MRL
384 was supported by the JPL Graduate Fellowship (JPLGF). MCL was supported in part by an
385 NSC grant 98-2111-M-001-014-MY3 to Academia Sinica. YLY was supported by NASA grant
386 NX09AB72G to the California Institute of Technology.

387

388

389

390 **REFERENCES**

391

392 Allen, M., Yung, Y. L., Waters, J. W. 1981, *J. Geophys. Res.*, 86, 3617-1627.

393

394 Burrows, A., Budaj, J., Hubeny, I. 2008, ApJ, 678, 1436-1457.
395
396 Burrows, A., Marley, M., Hubbard, W. B., Lunine, J. I., Guillot, T., Saumon, D., Freedman, R.,
397 Sudarsky, D., Sharp, C. 1997, ApJ, 491, 856-875
398
399 Bauerle, S., Klatt, M., Wagner, H.Gg. 1995, Ber. Bunsenges. Phys. Chem., 99, 870-879.
400
401 Baulch, D.L., Cobos, C.J., Cox, R.A., Esser, C., Frank, P., Just, Th., Kerr, J.A., Pilling, M.J.,
402 Troe, J., Walker, R.W., Warnatz, J. 1992, J. Phys. Chem. Ref. Data, 21, 411-429.
403
404 Charbonneau, D., Brown, T. M., Noyes, R. W., Gilliland, R. L. 2002, ApJ,
405 568, 377-384.
406
407 Cooper, C. S., Showman, A. P. 2006, ApJ, 649, 1048-1063
408
409 Fortney, J. J., Marley, M. S. 2007, ApJL, 666, L45-L48
410
411 Fortney, J. J., Marley, M. S., Lodders, K., Saumon, D., Freedman, R. 2005, ApJ, 627, 69-72.
412
413 Fortney, J. J., Saumon, D., Marley, M. S., Lodders, K., Freedman, R. S. 2006, ApJ, 642, 495-
414 504.
415
416 Fortney, J. J., Shabram, M., Showman, A. P., Lian, Y., Freedman, R. S., Marley, M. S., Lewis,
417 N. K. 2010, ApJ, 709, 1396-1406.
418
419 Friedson, A. J., Wilson, E. H., Moses, J. I. 2005, in DPS Conf. 37, #31.04 (Cambridge, UK)
420
421 Gladstone, G. R., Allen, M., Yung, Y. L. 1996, Icarus, 119, 1-52.
422
423 Gordon, S., McBride, B.J. 1994, Computer program for calculation of complex chemical
424 equilibrium compositions and applications. NASA Reference Publication 1311
425
426 Griffith, C. A., Yelle, R. V. 1999, ApJL, 519, L85-L88.
427
428 Kim, Y. H., Fox, J. L. 1994, Icarus, 112, 310-325
429
430 Liang, M.-C., Parkinson, C. D., Lee, A. Y.-T., Yung, Y. L., Seager, S. 2003, ApJL., 596, L247-
431 L250.
432
433 Liang, M.-C., Seager, S., Parkinson, C. D., Lee, A. Y.-T., Yung, Y. L. 2004, ApJL., 605, L61-
434 L64.
435
436 Madhusudhan, N., Seager, S. 2009, ApJ, 707, 24-39
437
438 Marley, M. S., Fortney, J. J., Hubickyj, O., Bodenheimer, P., Lissauer, J. J. 2007, ApJ, 655, 541-
439 549.

440
441 Moses, J. I., Fouchet, T., Bézard, B., Gladstone, G. R., Lellouch, E., Feuchtgruber, H., 2005, J.
442 Geophys. Res., 110 (E8)
443
444 O'Donovan, F. T., Charbonneau, D., Harrington, J., Madhusudhan, N., Seager, S., Deming, D.,
445 Knutson, H. A. 2010, ApJ, 710, 1551-1556
446
447 Page, M., Lin, M.C., He, Y., Choudhur, T.K. 1989, J. Phys. Chem., 93, 4404-4408.
448
449 Prinn, R. G., Barshay, S. S. 1977, Science, 198, 1031-1034.
450
451 Rogers, J. C., Apai, D., López-Morales, M., Sing, D. K., Burrows, A. 2009, ApJ, 707, 1707-
452 1716.
453
454 Sharp, C. M., Burrows, A. 2007, ApJS, 168, 140-166.
455
456 Segura, A., Krelove, K., Kasting, J. F., Sommerlatt, D., Meadows, V., Crisp, D., Cohen, M.,
457 Mlawer, E. 2003, Astrobiology, 3, 689-708.
458
459 Showman, A. P., Fortney, J. J., Lian, Yuan, Marley, M. S., Freedman, R. S., Knutson, H. A.,
460 Charbonneau, D. 2009, ApJ, 699, 564-584.
461
462 Smith, M. D. 1998, Icarus, 132, 176-184.
463
464 Srinivasan, N.K., Su, M.C., Sutherland, J.W., Michael, J.V., 2005, J. Phys. Chem. A, 109, 1857-
465 1863.
466
467 Swain, M. R., Vasisht, G., Tinetti, G., Bouwman, J., Chen, P., Yung, Y., Deming, D., Deroo, P.
468 2009a, ApJL., 690, L114-L117.
469
470 Swain, M. R., Tinetti, G., Vasisht, G., Deroo, P., Griffith, C., Bouwman, J., Chen, P., Yung, Y.,
471 Burrows, A., Brown, L. R., Matthews, J., Rowe, J. F., Kuschnig, R., Angerhausen, D. 2009b,
472 ApJ, 704, 1616-1621
473
474 Tinetti, G., Vidal-Madjar, A., Liang, M.-C., Beaulieu, J.-P., Yung, Y., Carey, S., Barber, R. J.,
475 Tennyson, J., Ribas, I., Allard, N., Ballester, G. E., Sing, D. K., Selsis, F. 2007, Nature, 448,
476 169-171.
477
478 Vidal-Madjar, A., Lecavelier des Etangs, A., Désert, J.-M., Ballester, G. E., Ferlet, R., Hébrard,
479 G., Mayor, M. 2003, Nature, 422, 143-146.
480
481 Visscher, C., Moses, J. I., Saslow, S. A. 2010, arXiv:1003.6077
482
483 Vuitton, V., Lavvas, P., Yelle, R. V., Galand, M., Wellbrock, A., Lewis, G. R., Coates, A. J.,
484 Wahlund, J.-E. 2009, P&SS, 57, 1558-1572.
485

486 Yung, Y. L., Allen, M., Pinto, J. P. 1984, ApJS, 55, 465-506.
487
488 Yung, Y.L., DeMore, W.B. 1999, Photochemistry of Planetary Atmospheres (Oxford University
489 Press)
490
491 Yung, Y. L., Drew, W. A., Pinto, J. P., Friedl, R. R. 1988, Icarus, 73, 516-526.
492
493 Zahnle, K., Marley, M. S., Freedman, R. S., Lodders, K., Fortney, J. J. 2009, ApJL., 701, L20-
494 L24.
495

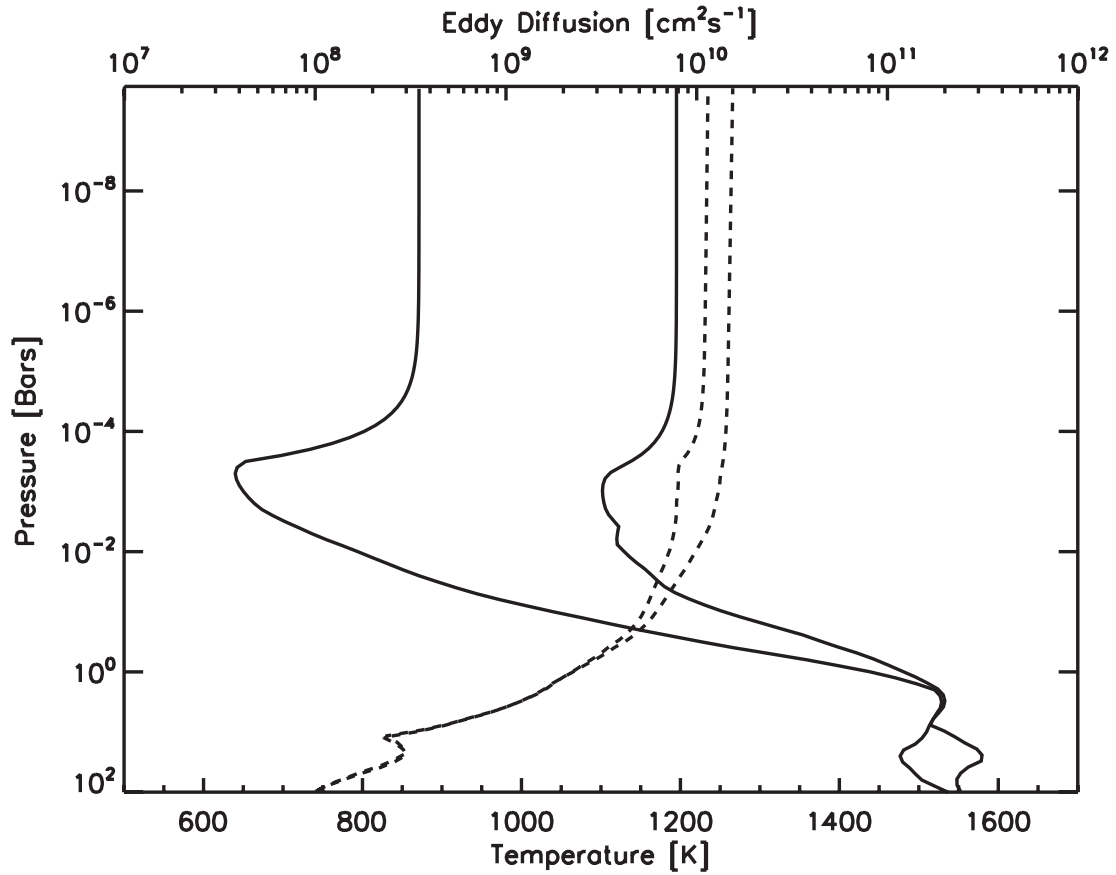


Figure 1. Temperature (solid) and eddy diffusion (dashed) profiles for the model atmosphere. The cooler temperature profile is taken from 30° N from the night side of the model by Showman et al., (2009). The hotter temperature profile is taken from the dayside at the same latitude. The larger eddy diffusion is estimated as discussed in the text (the larger values are for the dayside). Eddy diffusion is read along the top axis, temperature is read along the bottom axis.

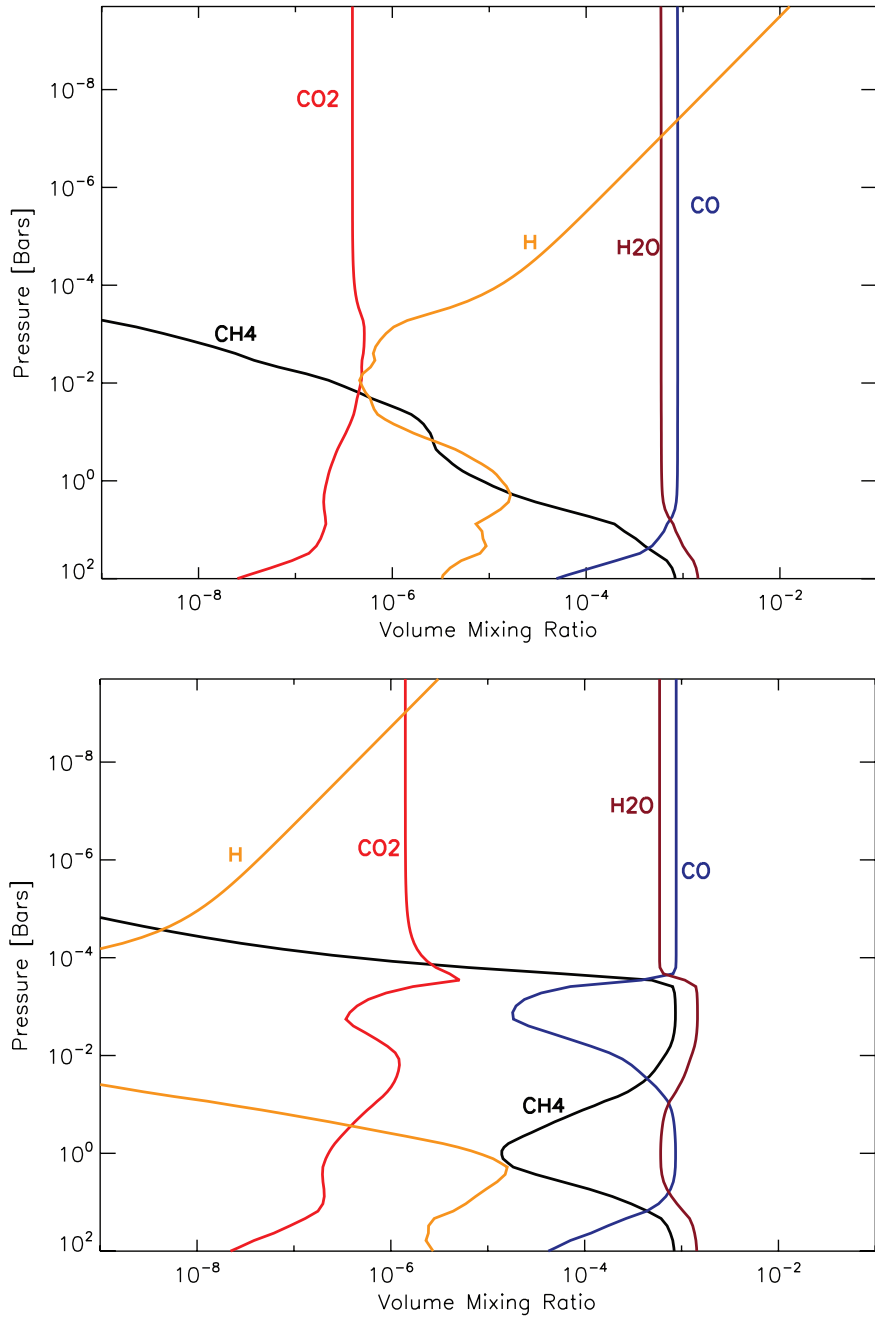


Figure 2. Thermochemical equilibrium mixing ratios derived from the temperature profiles in Figure 1. The top Figure shows the mixing ratios derived for the dayside (hotter) profile. The bottom Figure shows the mixing ratios derived for the (nightside) cooler profile.

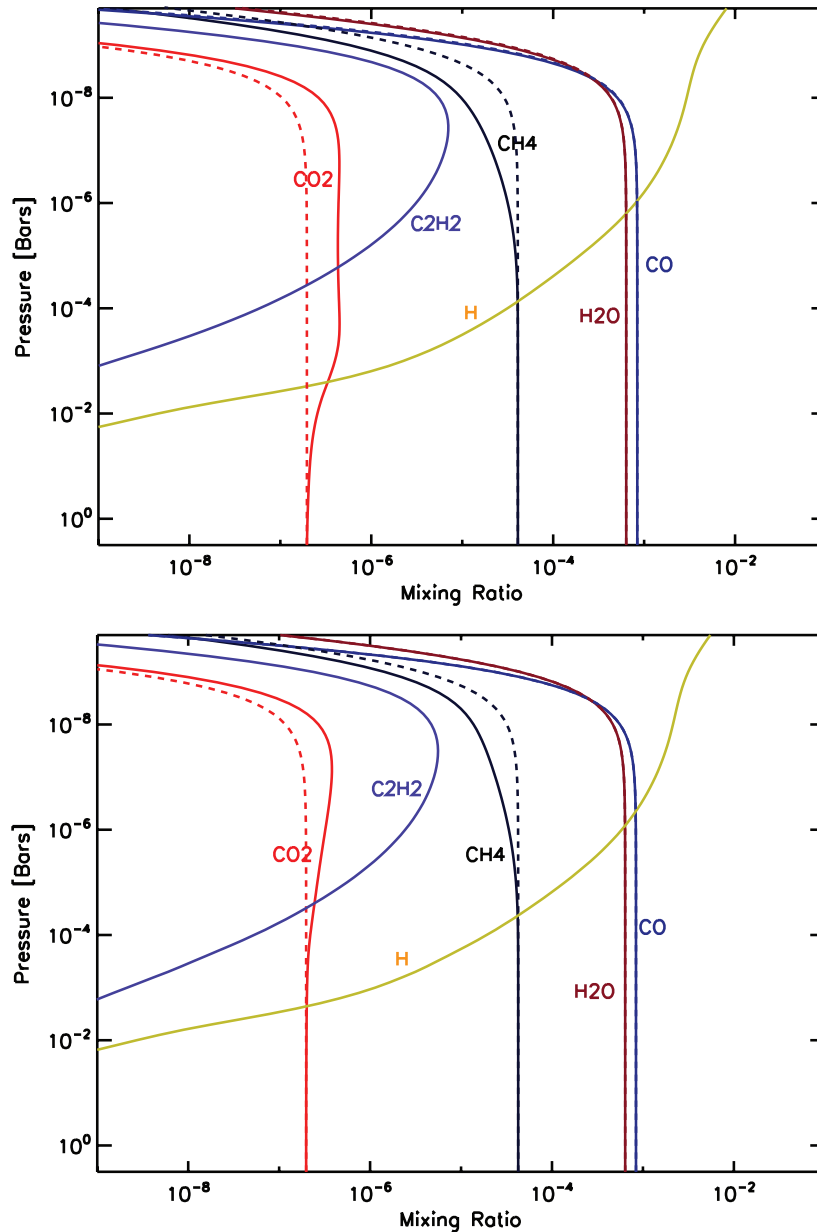


Figure 3. Photochemical mixing ratios (solid) compared to the case with no photochemistry and only quenching (dashed) for the day (top) and night (bottom) temperature profiles. The dashed curves on the bottom plot are representative of what may be seen on the night side of the planet. Note that there is virtually no H or C_2H_2 for the cases in which photochemistry is turned off (eg, the dashed curves for these species are not in the plot range).

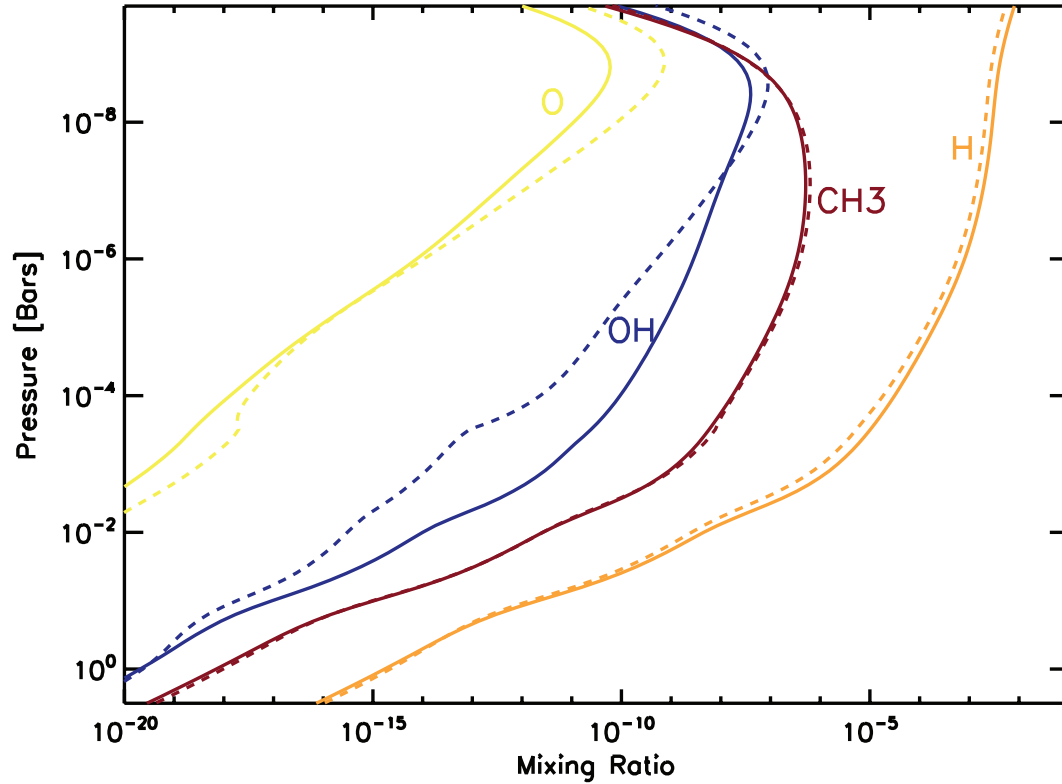


Figure 4. Important radical species involved in pathways governing the abundances of CH_4 , H_2O , CO and CO_2 . Solid is for the dayside temperature profile, dashed is for the nightside temperature profile. The abundances of radicals increase with decreasing pressure due to the availability of dissociating photons higher in the atmosphere.

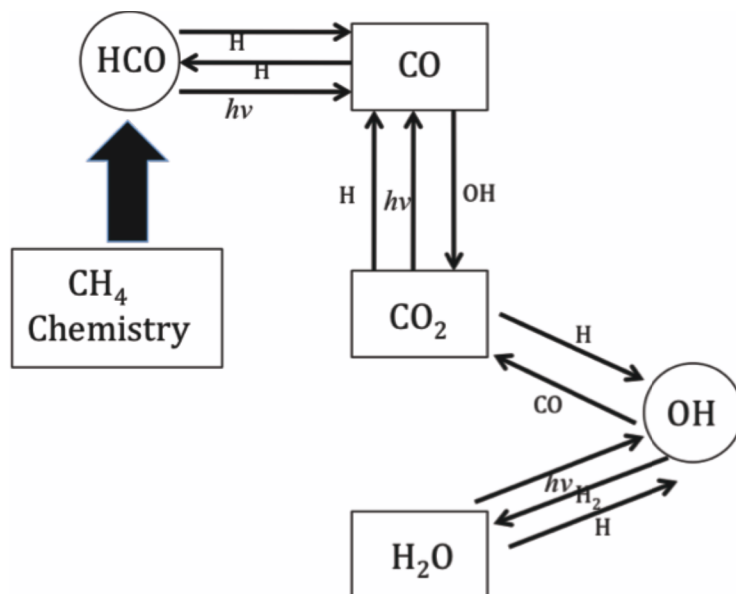


Figure 5. Photochemical web illustrating the important chemical pathways that govern the production and loss of the observable species. The boxes represent the observed species and the circles represent species yet to be observed but are key in the production and loss of the observed constituents.

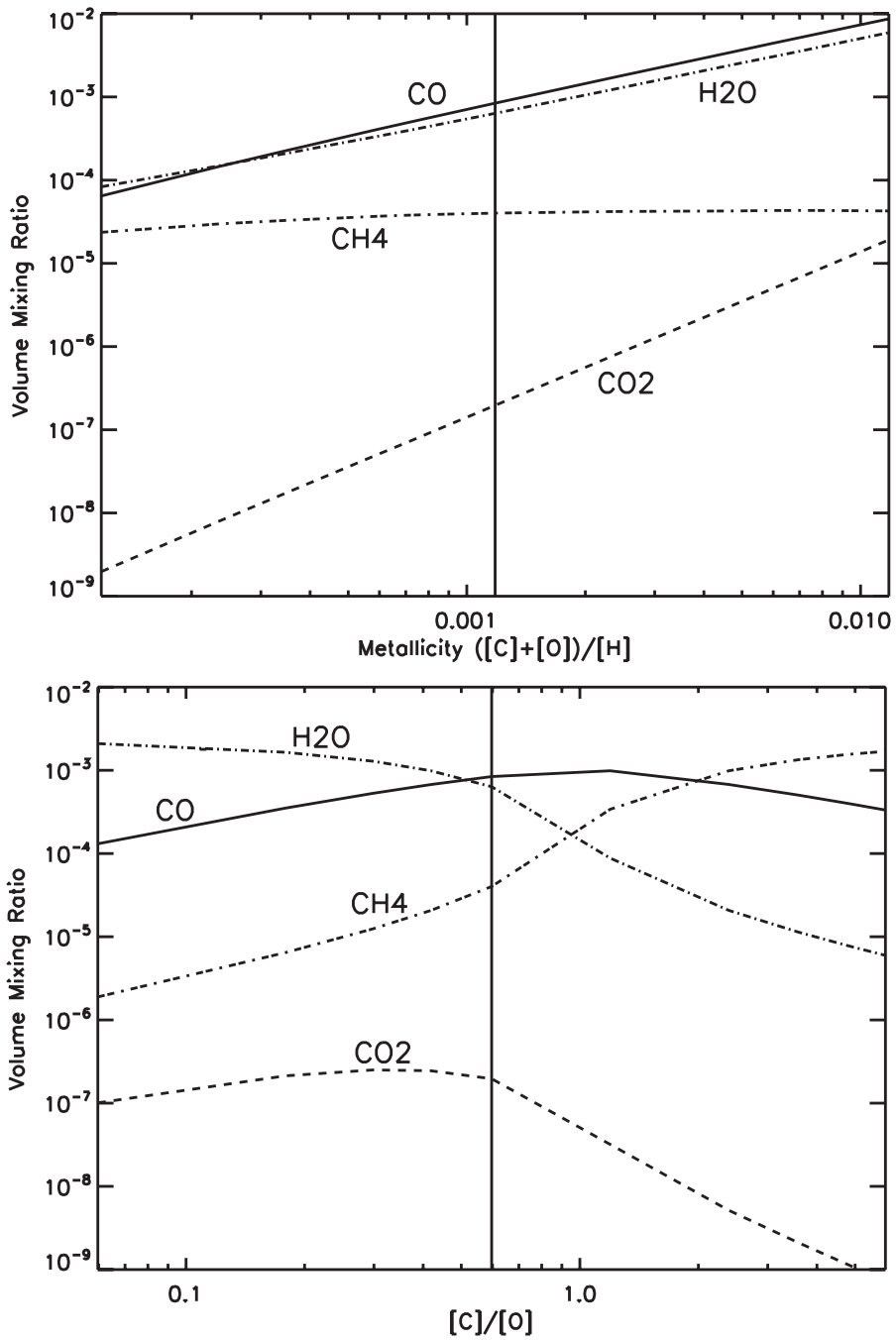


Figure 6. The effects of changing metallicity (top) and C/O ratio (bottom) on the 3 bar quench level mixing ratios for CO, H₂O, CO₂ and CH₄. The vertical lines in each plot represent the solar values.